Available online at www.sciencedirect.com
ScienceDirect
Journal of Catalysis 245 (2007) 369–380
JOURNAL OF CATALYSIS
www.elsevier.com/locate/jcat

Structural evolution of $H_4PVMo_{11}O_{40}\cdot xH_2O$ during calcination and isobutane oxidation: New insights into vanadium sites by a comprehensive in situ approach

A. Brückner [a,*,1], G. Scholz [b], D. Heidemann [b], M. Schneider [a], D. Herein [a], U. Bentrup [a], M. Kant [a]

[a] *Leibniz-Institut für Katalyse an der Universität Rostock e.V., Außenstelle Berlin, Richard-Willstätter-Str. 12, D-12489 Berlin, Germany*
[b] *Humboldt-Universität zu Berlin, Institut für Chemie, Brook-Tailor-Str. 2, 12489 Berlin, Germany*

Received 19 July 2006; revised 3 November 2006; accepted 6 November 2006

Available online 28 November 2006

Dedicated to Prof. Dr. Bernhard Lücke on the occasion of his 70th birthday

Abstract

$H_4PVMo_{11}O_{40}\cdot 8H_2O$ was studied during thermal activation as well as during isobutane oxidation by simultaneous in situ-EPR/UV–vis/Raman spectroscopy, in situ-FTIR spectroscopy, and quasi-in situ-^{1}H and -^{51}V-MAS-NMR. In as-synthesized form, most V sites are pentavalent, octahedrally coordinated, and located within the intact Keggin anions. Stepwise dehydration in N_2 up to 350 °C leads to partial reduction and disintegration of the V sites from the Keggin units, followed by their condensation on the outer surface of the latter in square-pyramidal form. In water-free $H_4PVMo_{11}O_{40}$, only V^{5+} (not V^{4+}) is stable inside the Keggin unit. Thus, disintegration of V from the latter is favored by its reduction to the tetravalent state and thus depends on the redox properties of the atmosphere. Active sites in isobutane oxidation are most likely composed of single $O_4V^{4+/5+}{=}O$ species connected to Mo^{6+} via oxygen bridges. Partial deactivation occurs by formation of carbon-containing deposits.

Keywords: Heteropoly acid; In situ spectroscopy; EPR; Raman; FTIR; XRD; Solid state NMR; Selective oxidation

1. Introduction

Vanadium-containing polyoxometallates with Keggin-type structure, particularly those consisting of $[PVMo_{11}O_{40}]^{4-}$ units ($PVMo_{11}$), and their salts have been revealed to be promising catalysts for the selective oxidation of various hydrocarbons, for example, for the oxidation of methacrolein (MAC) to methacrylic acid (MAA) [1–3], the oxidative dehydrogenation of isobutyric acid to MAA [4–7], and the direct oxidation of isobutane to MAC and MAA [8,9].

Both $H_3PMo_{12}O_{40}\cdot xH_2O$ (PMo_{12}) and $H_4PVMo_{11}O_{40}\cdot xH_2O$ ($PVMo_{11}$), as well as their salts, have been subject of a number of spectroscopic studies performed during or after thermal dehydration in a flow of air or inert gas, as well as during or after exposure to different reactive gases such as methanol [10–12], ethanol [10], propene [13–15], methacrolein [2,3], and mixtures of these gases with oxygen. The main aim of all these studies was to elucidate the nature of the active phase formed from the as-synthesized compounds during thermal treatment and equilibration under various atmospheres. Despite numerous earlier studies, this issue remains controversial. In the case of PMo_{12}, certain authors assume that Mo ions are expelled from the complex anions, leaving behind so-called lacunary Keggin units with one or more Mo defects [2,13,15]. However, the connection of two additional Mo atoms (released by thermal decomposition and amorphization of a part of PMo_{12}) to the remaining intact Keggin units, followed by formation of a new $(MoO_x)_{0.5}PMo_{14}O_{42}$ phase, has also been discussed. The catalytic activity in the oxidation of MAC has been attributed to the latter phase, whereby no information about the role of the amorphous material was given [3].

* Corresponding author. Fax: +49 30 6392 4454.
E-mail address: angelika.brueckner@catalysis.de (A. Brückner).
[1] Leibniz-Institut für Katalyse an der Universität Rostock e. V., Außenstelle Berlin, P.O. Box 96 11 56, D-12474 Berlin.

0021-9517/$ – see front matter
doi:10.1016/j.jcat.2006.11.004

In general, a higher catalytic performance in the selective oxidation of isobutane has been observed for $PVMo_{11}$ in comparison with its vanadium-free PMo_{12} counterpart [8]. This suggests that V might be part of the active site in $PVMo_{11}$. However, the structural evolution of those V sites during treatment in various atmospheres is uncertain. Quite a few papers have discussed the disintegration of V from the Keggin units and its transport into counterion positions between the remaining lacunary Keggin anions [4–6,9,11,12]. From in situ-XRD measurements, it was concluded that a vanadyl salt of the water-free heteropolyacid is formed during selective oxidation of isobutyric acid [5]. However, it has also been claimed that it is not the V, but rather the Mo ions that are disintegrated from the $PVMo_{11}$ Keggin unit and move into cation positions, forming a cubic $Mo_x[PVMo_{11-x}O_{40}]$ salt, which is believed to be the carrier of catalytic activity in propene oxidation [14]. In the ideal $H_4PVMo_{11}O_{40}\cdot xH_2O$ structure, with all metal atoms being part of the Keggin anion, Mo and V should exist in their highest oxidation states. However, in most real $PVMo_{11}$ materials, a certain amount of reduced VO^{2+} species is detected [4,12,16]. Moreover, XAS, UV–vis and EPR studies have shown that a marked reduction of Mo^{6+} and/or V^{5+} occurs under particular reaction conditions [11,12,14,15], the degree of which depends on the reducing agent. For example, methanol was found to be much more reducing than ethanol [10].

From ^{31}P ENDOR and HYSCORE measurements, it has been derived that reduced VO^{2+} species are not part of the Keggin anions, because the V^{4+}–P distance of 0.68 nm is too long [16]. It was concluded that VO^{2+} is located in the structural voids between the latter in the parent hydrated form and condenses on the surface of the Keggin units on dehydration. However, it remains an open question as to whether the V^{4+} detected under various reaction atmospheres arises from reduction of V^{5+} on disintegration from the Keggin units under these conditions or from reduction of V^{5+} that was never incorporated into the complex anions, even in the as-synthesized $PVMo_{11}$. As for V^{4+}, evidence for the incorporation of V^{5+} in the Keggin anions is not doubtless. Thus, an anisotropic ^{51}V-NMR signal with components at −314 and −971 ppm has been attributed to octahedral V^{5+} inside the Keggin anion of as-synthesized $PVMo_{11}$ [6]. It disappeared on calcination in air at 320 °C in favour of an isotropic line at −668 ppm assigned to tetrahedral V^{5+} outside the Keggin units, which was taken as an evidence for the disintegration of V^{5+} from the latter during calcination. Other attempts to identify V as part of the complex anion in $PVMo_{11}$ are based on IR measurements revealing a split band for the P–O stretching vibration in as-synthesized $PVMo_{11}$ that turned into a single band on calcination [9].

Given that vanadium is an initial constituent of the $PVMo_{11}$ Keggin anion and becomes disintegrated on thermal treatment/reduction, the stability of the latter will be crucially related to the reduction potential of the reaction mixture, which might differ markedly depending on the hydrocarbon. Thus, a generalization of the behaviour of $PVMo_{11}$ during selective oxidation of different hydrocarbons would be doubtful. As mentioned above, $PVMo_{11}$ belongs to the most effective catalysts for direct oxidation of isobutane to methacrolein and methacrylic acid but suffers from rapid deactivation [8,9]. This reaction is interesting from an industrial standpoint, because it is a one-step process based on an inexpensive feedstock and has negligible environmental impact. It could be an attractive alternative to the traditional acetone-cyanohydrin process, which comprises several steps and is environmentally harmful due to toxic raw materials, and the stoichiometric production of NH_4HSO_4 as an undesired side product. Against this background, it is surprising that almost no in situ studies have been reported on the behaviour of $PVMo_{11}$ under selective isobutane oxidation conditions, which might deviate from those of other hydrocarbons due to different reduction potentials, as mentioned above.

The aim of this work is to gain deeper insight into the structural evolution of V species being most likely part of the active site in $H_4PVMo_{11}O_{40}\cdot xH_2O$ in the partial oxidation of isobutane. Therefore, $PVMo_{11}$ was studied during the latter reaction as well as during activation in N_2 and air for the first time with the novel simultaneous in situ EPR/UV–vis/Raman/on line-GC technique [17], which provides information on structural changes of the catalyst by three spectroscopy measurements obtained simultaneously in a single experiment. In addition, in situ-FTIR spectroscopic investigations and ^{51}V- and ^{1}H-MAS-NMR studies of as-synthesized and calcined samples were performed to elucidate the active state of $PVMo_{11}$.

2. Experimental

$H_4PVMo_{11}O_{40}\cdot xH_2O$ was prepared from MoO_3, V_2O_5, and 85% phosphoric acid as described elsewhere [18]. Briefly, 22.3 g of MoO_3 and 1.3 g of V_2O_5 were added to 350 ml of deionized water, and the mixture was heated to reflux. Then 1.7 g of 85% phosphoric acid was added in three equal aliquots, followed by 150 ml of deionized water. After 15 h of reflux with vigorous stirring, the insoluble oxides had dissolved, and a deep-orange solution was formed. The liquid was evaporated, and a bright-orange solid was obtained. Thermal analysis (Netzsch STA 409; heating rate, 10 K/min; 50 ml/min N_2) revealed that the crystal water content was 8 H_2O. The water content was calculated from the mass loss during the first TG step between 100 and 250 °C, which is due to the release of crystal water.

For the in situ FTIR investigations, the sample was dispersed in ethanol and coated on an infrared transparent Si wafer (1 mm thick, 18 mm in diameter). During this manipulation, the orange colour of the sample remained unchanged, suggesting that the sample was not reduced in ethanol suspension. The wafer was placed in a heatable and evacuable IR cell with KBr windows, connected to a gas dosing/evacuation system, and heated in air or 20% isobutane/N_2 flow (40 ml/min) at a rate of 5 K/min. The spectra were recorded with a resolution of 2 cm^{-1} over 100 scans, using a Bruker IFS 66 spectrometer. Then the spectra of the pure Si wafer at appropriate temperatures were subtracted.

In situ EPR, UV–vis, and Raman spectra during calcination in N_2 or air flow and during treatment in a reactant atmosphere were recorded simultaneously as described in detail elsewhere [17]. Briefly, an UV–vis fibre optical sensor connected to an AVASPEC fibre optical UV–vis spectrometer

(Avantes) was introduced into an EPR fixed-bed flow reactor located within the rectangular X-band cavity of an ELEXSYS 500-10/12 cw-spectrometer (Bruker), and the beam of a 785 nm diode laser of a Kaiser Optical Systems RXN spectrometer was focused through a front hole in the EPR cavity onto the catalyst bed within the reactor. EPR spectra were recorded with a microwave power of 6.3 mW, a modulation frequency of 100 kHz, and a modulation amplitude of 0.5 mT. Raman spectra were measured with a laser power of 8 mW and an acquisition time of 3 s. Five scans were accumulated for each spectrum. Computer simulation of EPR spectra was performed with the program SIM14S of Lozos et al. [19] using the spin Hamiltonian,

$$H = \mu_B \cdot S \cdot g \cdot B_0 + SAI, \quad (1)$$

in which μ_B is the Bohr magneton, S is the electron spin operator, g is the g tensor, B_0 is the magnetic field vector, A is the hyperfine tensor, and I is the nuclear spin operator. For thermal pretreatment, 100 mg of catalyst particles (250–355 μm) were heated at a rate of 3 K/min in N_2 or air flow (10 ml/min) to 350 °C. For monitoring the behavior of the catalyst under working conditions, spectra were recorded either during stepwise heating of the pretreated catalyst from 20 to 350 °C in a flow of 11% isobutane and 17% O_2/N_2 (total flow, 1.6 ml/min) with a 10 min isothermal hold at each temperature for recording spectra and gas chromatograms, or as a function of time after switching to the feed flow at 350 °C. The isobutane conversion was determined on-line by a GC 17AAF capillary gas chromatograph (Shimadzu) equipped with a flame ionization detector.

The concentration of VO^{2+} in selected samples was determined by comparing the double integrals of the EPR signals with those of a spin standard (mechanical mixture of $VOSO_4$ and K_2SO_4) using a rectangular double cavity. As determined separately by potentiometric titration, this spin standard contains $3.98 \cdot 10^{20}$ spins/g.

X-ray powder diffraction patterns were recorded using a Theta/Theta diffractometer (Seifert/FPM) with Bragg-Brentano geometry and a multilayer mirror to maximize the diffracted intensity of Cu$K\alpha$ radiation. The XRD patterns were scanned in the 2θ range of 5°–45° (step width 0.02°, 5 s/step) and recorded with a scintillation counter. Data interpretation was carried out using the WinXpow (STOE) software, and the database of the Powder Diffraction File (PDF) of the International Centre of Diffraction patterns was performed by the Data (ICDD).

Calculation of XRD powder patterns was done with the programs Powdercell 2.4 and Cerius^2 (Accelrys). The single-crystal structure of $H_3PMo_{12}O_{40}\cdot 13H_2O$ [20] was used as input data. The interstitial position of the $VO(H_2O)_x^{n+}$ species of the theoretical $[VO(H_2O)_n]H_xPMo_{12}O_{40}\cdot 13H_2O$ structure was determined as follows. First, all H_2O molecules were removed; then the total free space between the Keggin units was calculated. A $VO(H_2O)_4$ species with square pyramidal symmetry was placed in the middle of the maximum available interstitial space between the Keggin units. The crystallographic coordinates for the vanadium atom were near $(x, y, z) = (0.61, 0.71, 0.405)$.

^1H and ^{51}V MAS NMR spectra were recorded on a Bruker AVANCE 400 spectrometer (Larmor frequencies: $\nu_{1H} = 400.1$ MHz and $\nu_{51V} = 105.2$ MHz) using 4 and 2.5-mm magic angle spinning (MAS) probes (Bruker Biospin). ^{51}V MAS NMR ($I = 7/2$) spectra were recorded with an excitation pulse duration of 0.6 μs, ensuring a linear irradiation regime to reduce the distortion of the spectra. $VOCl_3$ was used as a reference for the chemical shift of ^{51}V. The recycling delay was 1 s, and the accumulation number was 3600 for the 4-mm probe. The measurement at 25 kHz was performed with a recycling delay of 0.2 s and required an accumulation number of 400,000 to obtain a reasonable signal to noise ratio.

^1H MAS NMR spectra were measured with a sweep width of 100 kHz, an excitation pulse length of 2.7 μs, and a recycling delay of 60 s. For the $\pi/2$ pulse experiments, existent background signals of ^1H could be completely suppressed with the application of a phase-cycled depth pulse sequence according to Cory and Ritchey [21]. The ^1H MAS NMR spectra were calculated using the DMFIT program [22]. For the NMR measurements, as-synthesized $PVMo_{11}$ was heated to 100 or 300 °C in air flow to prevent an overly strong reduction to paramagnetic V^{4+}, which would disturb the NMR measurement. After cooling to room temperature, the samples were filled into the probes within a glove box to avoid rehydration.

3. Results

3.1. XDR studies

Fig. 1 shows the experimental X-ray diffraction pattern obtained from the untreated $H_4PVMo_{11}O_{40}\cdot 8H_2O$ starting material together with the calculated powder XRD pattern obtained from the single-crystal data of $H_3PMo_{12}O_{40}\cdot 13H_2O$ [20]. The calculated XRD pattern was adapted to the main reflections of the experimental pattern at 5°–10° 2θ and led to an acceptable overall agreement between experiment and simulation suggesting that the V-containing 8-hydrate studied in this work can be described by the same triclinic space group adopted by the V-free 13-hydrate. However, the exact crystallographic unit cell parameters of the starting $H_4PVMo_{11}O_{40}\cdot 8H_2O$ material cannot be determined simply by powder X-ray diffraction. The model compound $H_3PMo_{12}O_{40}\cdot 13H_2O$ used for simulation of the XRD pattern crystallizes in the triclinic space group P-1 (no. 2) with three independent unit cell axes and unit cell angles. Thus, in general, powder XRD does not provide sufficient independent observations to allow determination of triclinic crystal systems. This uncertainty in the unit cell parameter determination is the reason for the difference between experimental and simulated XRD patterns (Fig. 1a) and does not allow precise verification of the crystal structure of as-synthesized $H_4PVMo_{11}O_{40}\cdot 8H_2O$ by merely a simple comparison of the experimental data with the known single-crystal structure of $H_3PMo_{12}O_{40}\cdot 13H_2O$ using the Rietfeld method.

To explore whether or not as-synthesized $H_4PVMo_{11}O_{40}\cdot 8H_2O$ contains interstitial $VO(H_2O)_x^{n+}$ species, the single-

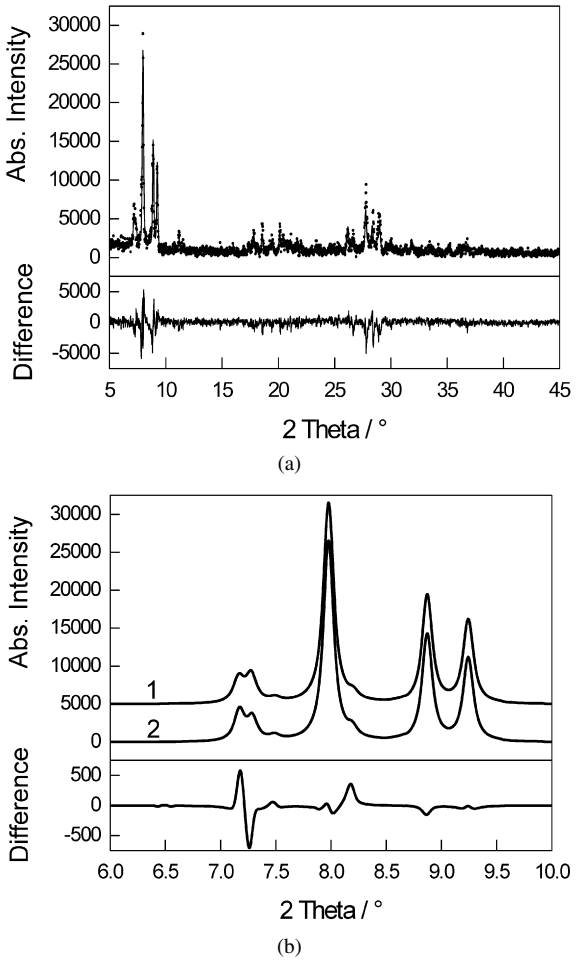

Fig. 1. XRD powder patterns of as-synthesized $H_4PVMo_{11}O_{40}\cdot 8H_2O$: (a) experimental (points) and calculated (line) assuming all V atoms as part of the Keggin units; (b) comparison of calculated patterns in the range of the strongest reflections assuming all V atoms within (2) and outside the Keggin units (1).

crystal structure of $H_3PMo_{12}O_{40}\cdot 13H_2O$ with its original unit cell parameters was used to calculate XRD patterns. Fig. 1b compares calculated XRD powder patterns of $H_3PMo_{12}O_{40}\cdot 13H_2O$ (trace 2) and $[VO(H_2O)_n]H_xPMo_{12}O_{40}\cdot 13H_2O$ (trace 1). It can be seen that the difference in the peak intensities caused by placing additional $VO(H_2O)_x^{n+}$ species in the void space between the Keggin units is so small that it cannot be distinguished from the scatter of the experimental data in Fig. 1a. Thus, clearly the question of whether the V atoms are located inside or outside the Keggin units cannot be answered by XRD; other, more sensitive techniques are needed to solve this problem.

3.2. Simultaneous EPR/UV–vis/Raman studies

3.2.1. Measurements of as-synthesized $H_4PVMo_{11}O_{40}\cdot 8H_2O$ at room temperature

Before the catalytic experiments, $H_4PVMo_{11}O_{40}\cdot 8H_2O$ was heated in N_2 to 350 °C. Spectra recorded during this process at selected temperatures are shown in Figs. 2–4. The experimental EPR spectrum at 20 °C before any treatment shows the characteristic signal of isolated VO^{2+} species with hyperfine structure (hfs) (Fig. 2, solid line). Spin concentration measurements revealed that this signal composes 2.3% of the total V content in the sample. Spin Hamiltonian parameters derived by spectra simulation (Fig. 2, dashed line; Table 1) account for axial g and A tensors and are close to those obtained for $[VO(H_2O)_5]^{2+}$ in a frozen aqueous solution [12] and to those obtained for $[VO(H_2O)_5]H[PMo_{12}O_{40}]\cdot 23H_2O$ at low temperature, in which the $[VO(H_2O)_5]^{2+}$ ions are known to be located in cation positions outside the Keggin units [23]. A VO^{2+} signal with very similar spin Hamiltonian parameters was also observed in $H_4PVMo_{11}O_{40}\cdot 32H_2O$ [16]. From the P–V^{4+} distance of 0.68 nm derived by ^{31}P ENDOR it has

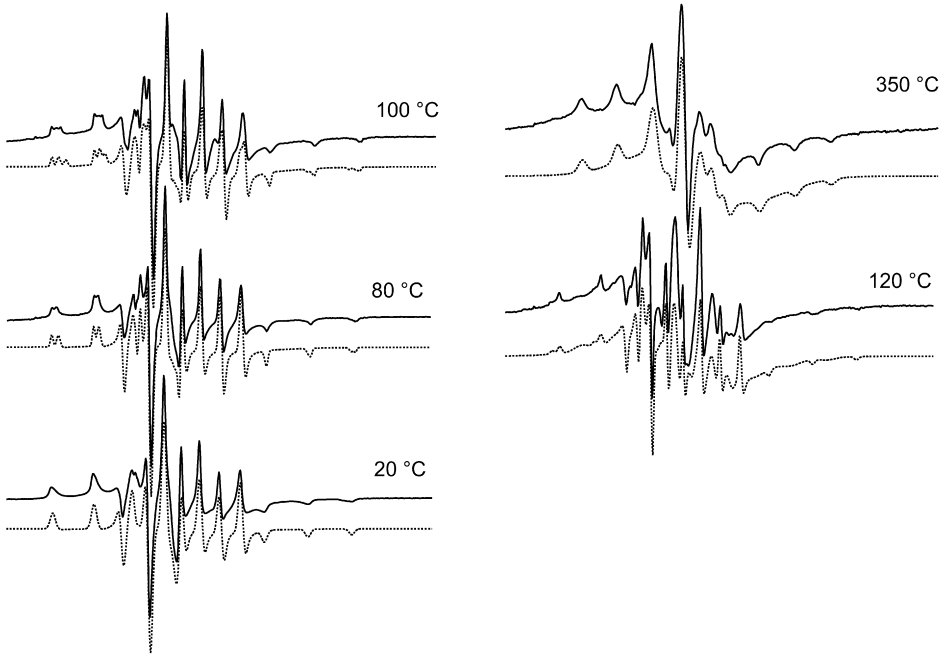

Fig. 2. Experimental (—) and calculated (···) EPR spectra measured during heating of $H_4PVMo_{11}O_{40}\cdot 8H_2O$ in N_2 flow.

Table 1
Spin Hamiltonian parameters derived by simulation of selected EPR spectra of $H_4PVMo_{11}O_{40}\cdot 8H_2O$ during heating in N_2 flow

Spectrum	Species	$g_\parallel$	$g_\perp$	$A_\parallel$ (10^{-4} cm^{-1})	$A_\perp$ (10^{-4} cm^{-1})	$\Delta g_\parallel/\Delta g_\perp$	$A_\parallel/A_\perp$	$g_\perp - g_\parallel$	β_2^{*2}	I_{rel} (%)
20 °C	A	1.936	1.986	−188	−75	4.07	2.51	0.050	0.96	100
80 °C	A	1.932	1.984	−192	−75	3.84	2.56	0.052	0.99	30
	B	1.928	1.983	−185	−75	3.85	2.47	0.055	0.92	37
	E	1.971	1.971	–	–					33
100 °C	A	1.932	1.982	−192	−75	3.46	2.56	0.050	1.04	17
	B	1.928	1.986	−185	−75	4.55	2.47	0.058	0.92	21
	C	1.928	1.986	−177	−70	4.55	2.53	0.058	0.89	14
	E	1.962	1.962	–	–					48
350 °C	D	1.930	1.965	−154	−40	1.94	3.85	0.035	0.97	23
	E	1.941	1.941	–	–					77

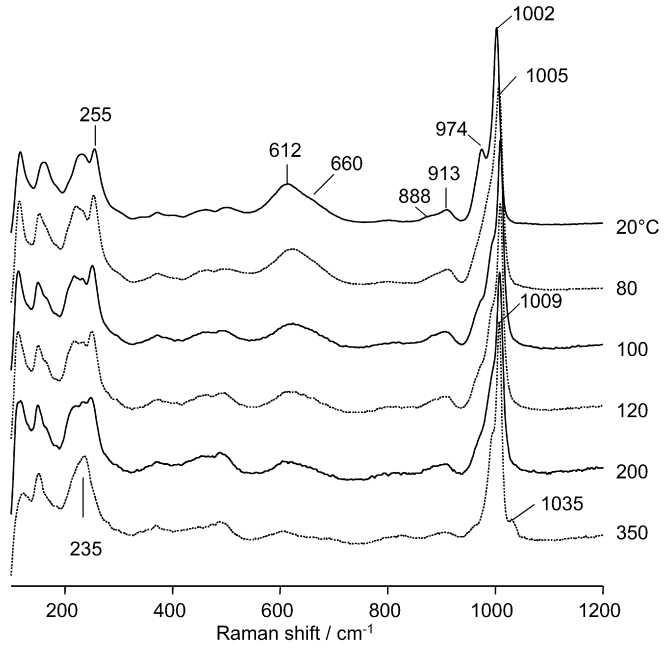

Fig. 3. Raman spectra measured during heating of $H_4PVMo_{11}O_{40}\cdot 8H_2O$ in N_2 flow in parallel with the EPR spectra of Fig. 2.

been convincingly concluded that these sites cannot be part of the Keggin units but rather are located as $[VO(H_2O)_5]^{2+}$ in the void space between the latter. Due to the similarity of the spin Hamiltonian parameters with the previously reported values [16,23], we assign the EPR signal in the initial 8-hydrate studied in this work to VO^{2+} sites outside the Keggin units. In contrast to $[VO(H_2O)_5]H[PMo_{12}O_{40}]\cdot 23H_2O$ and $H_4PVMo_{11}O_{40}\cdot 32H_2O$, for which hfs anisotropy is lost at room temperature due to the rapid tumbling of the $[VO(H_2O)_5]^{2+}$ ions [16,23], the hfs signal of the 8-hydrate remains anisotropic at room temperature (Fig. 1). This may be due to the markedly lower water content, which causes a narrowing of the void space between the Keggin units. As a consequence, the free tumbling of the $[VO(H_2O)_5]^{2+}$ species in $H_4PVMo_{11}O_{40}\cdot 8H_2O$ may be suppressed.

The Raman bands observed for $H_4PVMo_{11}O_{40}\cdot 8H_2O$ at 20 °C (Fig. 3) can be assigned to the following vibrations [13]: ν(Mo=O) at 1002 and 974 cm^{-1}; ν(Mo–O) at 913, 888, 612, and 660 cm^{-1}; and δ(Mo–O–Mo) at 256 and 235 cm^{-1}. The bands at 1005, 888, 612, and 256 cm^{-1} arise from the intact Keggin units, whereas the bands at 974, 913, 660 (sh), and 235 cm^{-1} have been assigned to defective Keggin anions formed on disintegration of a MoO_6 or VO_6 octahedron [13].

The UV–vis spectrum at 20 °C shows strong absorbance below 600 nm arising from charge-transfer (CT) transitions between oxygen ligands and Mo^{6+} and V^{5+} metal ions [24] (Fig. 4a). The weak broad band with a maximum between 700 and 800 nm is due to d–d transitions of reduced V^{4+} [24]. Generally, reduced Mo^{5+} should give rise to a d–d band in the same range; however, no evidence for the presence of Mo^{5+} has been found by EPR.

3.2.2. Thermal dehydration

On stepwise heating in N_2 flow, two additional EPR hfs signals, B and C, appear at 80 and 100 °C, respectively (Fig. 2, Table 1). More information about their structure can be obtained by evaluating the spin Hamiltonian parameters in Table 1. The parameter $\Delta g_\parallel/\Delta g_\perp$ (with $\Delta g_\parallel = g_\parallel - g_e$ and $\Delta g_\perp = g_\perp - g_e$) characterizes the overall extent of axial distortion of the V^{4+} site. The larger the $\Delta g_\parallel/\Delta g_\perp$, the higher the distortion, that is, the shorter the V=O bond and the longer the four V–O bonds within the equatorial plane [25,26]. β_2^{*2} is the in-plane delocalization coefficient. It is a measure of the extent to which the unpaired electron of the V^{4+} is delocalized toward the four oxygen ligands within the basal plane of the VO^{2+} species, that is, a measure of the degree of covalency of the V–O bonds. $\beta_2^{*2} = 1$ when the unpaired electron is completely localized at the V^{4+} nucleus, that is, when the ionic character is highest. β_2^{*2} can be calculated using Eq. (1), in which $P = 128$ cm^{-1} for the free V^{4+} ion is used [25]:

$$\beta_2^{*2} = \frac{7}{6}\left(\Delta g_\parallel - \frac{5}{14}\Delta g_\perp - \frac{A_\parallel - A_\perp}{P}\right) \quad (1)$$

β_2^{*2} is very close to unity for signal A, reflecting $[VO(H_2O)_5]^{2+}$ cations. Although β_2^{*2} decreases slightly for signals B and C, it still suggests an almost pure ionic character of the respective VO^{2+} species. The quantities $\Delta g_\parallel/\Delta g_\perp$, $A_\parallel/A_\perp$, and $g_\perp - g_\parallel$ of hfs signals A–C are all rather similar and within the range

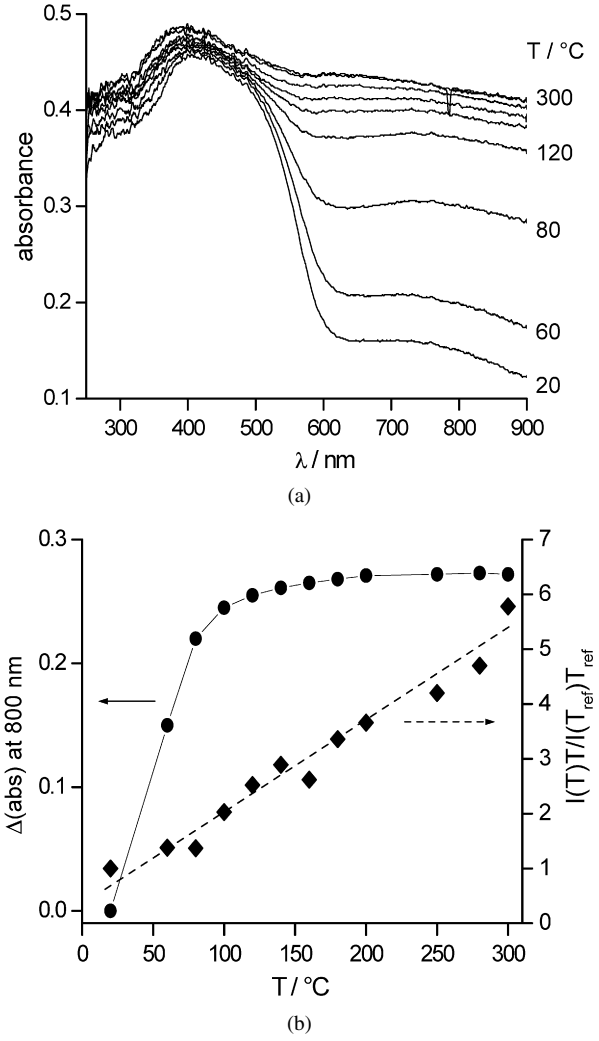

Fig. 4. (a) UV–vis spectra measured during heating of $H_4PVMo_{11}O_{40}\cdot 8H_2O$ in N_2 flow in parallel with the EPR spectra of Fig. 2 and the Raman spectra of Fig. 3; (b) difference of absorbance at 800 nm of the UV–vis spectra in comparison to the double integral of the EPR spectra measured in parallel as a function of temperature during heating in N_2 flow.

expected for distorted octahedral coordination [25,26]. Above 200 °C, signals A–C disappear in favour of a new hfs line D, which remains unchanged until 350 °C (Fig. 2). The values of $\Delta g_\parallel/\Delta g_\perp$, $A_\parallel/A_\perp$, and $g_\perp - g_\parallel$ differ markedly from those of signals A–C and are characteristic for square-pyramidal VO^{2+} species [25,26]. Very similar values have also been found for VO^{2+} ions in Rochelle salt, which are known to take square pyramidal symmetry [25]. The β_2^{*2} value of this signal is still very close to unity. As for VO^{2+} species A–C, this points to the almost pure ionic character of species D and suggests that all four V^{4+} species might be located outside the Keggin units, where they could take the role of counterions.

With increasing temperature, the overall EPR intensity, $I(T)T/I(T_{ref})T_{ref}$ (double-integral normalized on a reference temperature to eliminate the influence of temperature according to the Curie–Weiss law) rises linearly (Fig. 4b). This is due to further reduction of VO^{3+} to VO^{2+} and agrees with the observation of additional EPR signals. The broad isotropic signal E, which is due to VO^{2+} sites with weak dipolar interaction, must be superimposed at elevated temperature to obtain a good fit of the experimental EPR spectrum (Fig. 2, Table 1). Besides higher V^{4+} concentration, the latter might be caused by decreasing mean distances between the metal ions in the crystal unit cell due to the loss of crystal water [24]. Comparison of the EPR intensity (double integral) with that of the $VOSO_4/K_2SO_4$ spin standard reveals that after calcination in N_2, the amount of VO^{2+} increases by a factor of 5.6 to 12.9% of the total V content. When calcination is done in air instead of N_2 flow, the same spectral changes are observed, but the total intensity of the EPR spectrum is slightly lower, because the reduction of V^{5+} to V^{4+} may be less favoured.

In the Raman spectra, the ν(Mo=O) vibration is successively shifted to higher wavenumbers with the loss of crystal water at higher temperatures. This is due to desorption of water molecules bound to the terminal Mo=O groups of the Keggin units in the hydrated heteropoly compound [13]. The δ(Mo–O–Mo) band of the intact Keggin units at 255 cm^{-1} remains unchanged up to 200 °C and shifts to 235 cm^{-1} (assigned to δ(Mo–O–Mo) of defective Keggin units) above this temperature. Simultaneously, a small band appears at 1035 cm^{-1} that is generally attributed to the ν(V=O) vibration of dehydrated VO_x species [27–29].

In the UV–vis spectra, light absorption above 600 nm increases strongly with rising temperature (Fig. 4a). In partially reduced $H_4PVMo_{11}O_{40}\cdot xH_2O$, this range is dominated by V^{4+}–O–Mo^{6+} and/or V^{5+}–O–Mo^{5+} intervalence charge-transfer (ICVT) transitions, which are more intense than d–d transitions [24]. Because Mo^{5+} formation could not be detected by EPR (Fig. 2, Table 1), the increase of absorbance above 600 nm in the UV–vis spectra of Fig. 4a is attributed mainly to V^{4+}–O–Mo^{6+} ICVT transitions, along with a weak contribution of V^{4+} d–d transitions. In contrast to the linearly rising EPR intensity, reflecting the amount of V^{4+} only, the increase of absorbance in the UV–vis spectra is much more pronounced in the lower temperature range in which the crystal water is released (Fig. 4b). This is due to a combined effect of dehydration and V reduction and can be discussed in terms of a shortening of the distance between the Mo^{6+} and the V^{4+} ions with the removal of crystal water, which facilitates the electron transfer between the latter [24].

3.2.3. Treatment under catalytic conditions

When the calcined $H_4PVMo_{11}O_{40}$ is heated in a flow of 11% isobutane and 17.7% O_2/N_2, the spin Hamiltonian parameters of the EPR hfs signal D do not change (Fig. 5a); however, its normalized total intensity increases up to 350 °C and then remains constant during time on stream (Fig. 5c). This agrees nicely with the behaviour of UV–vis absorbance above 600 nm (Figs. 5b and 5d) and points to a further reduction of vanadyl species during thermal treatment in reactant flow. After 2 h under reaction conditions, an increase of the total EPR intensity by a factor of 2.5 is observed (Fig. 5c), but no Mo^{5+} is detected. This means that after reaction, about 32% of the total V is reduced to V^{4+}. This demonstrates that the *i*-butane/O_2/N_2 feed has much weaker reducing properties compared with the

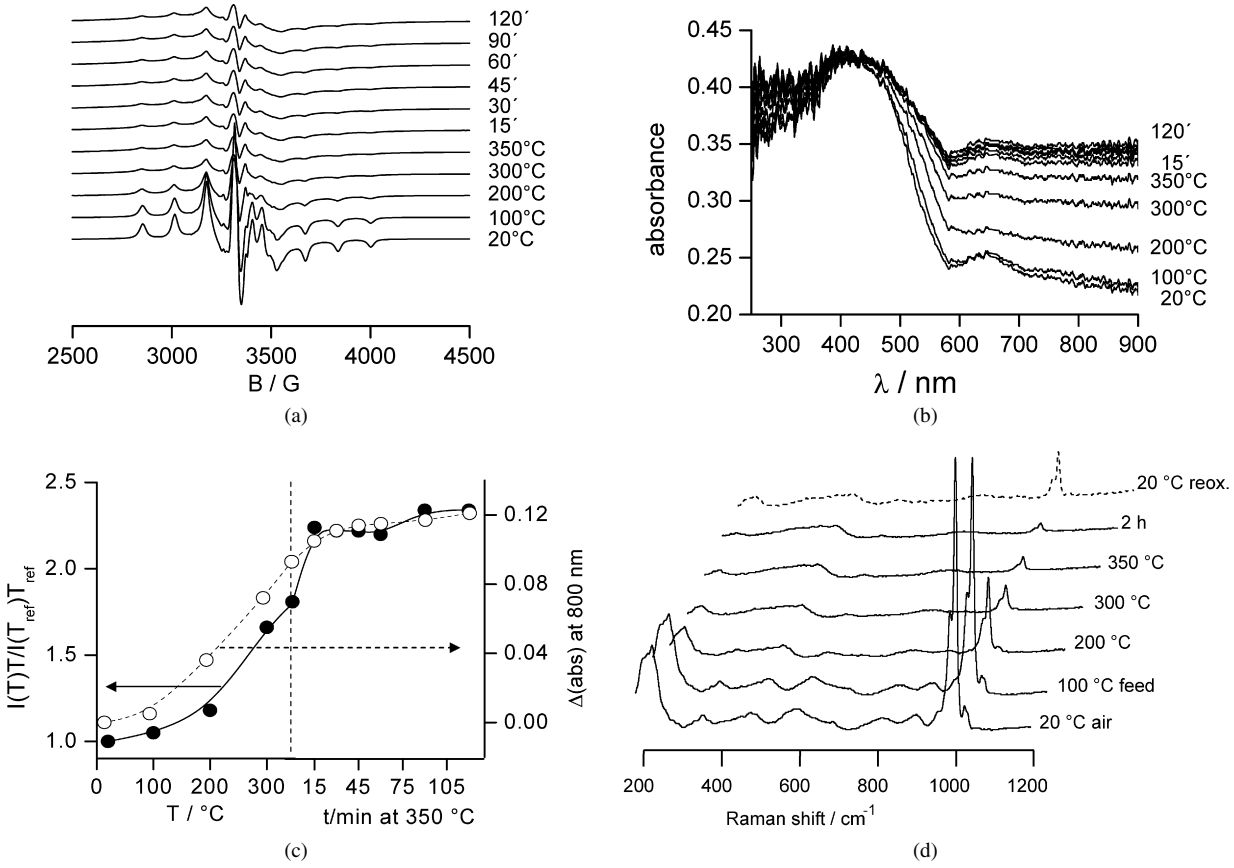

Fig. 5. In situ-EPR (a), -UV–vis (b) and -Raman spectra (d) during heating of dehydrated $H_4PVMo_{11}O_{40}$ in a flow of 11% *i*-butane, 17% O_2/N_2 and comparison of the difference of absorbance at 800 nm of the UV–vis spectra with the double integral of the EPR spectra (c).

feed used for methanol oxidation in which a complete reduction of V^{5+} to V^{4+} was observed [12]. Increasing V reduction goes along with the total disappearance of the ν(V=O) band in the Raman spectra (Fig. 5d). Note that this band arises from pentavalent V^{5+}=O species only. VO^{2+} species as evidenced by EPR are hardly visible in Raman spectra [27]. Moreover, the darkening of the sample due to V reduction leads to an overall decrease of the Raman intensity. At 350 °C, an isobutane conversion of 2% is measured, which passes a maximum after 40 min time on stream and then decreases again slightly (Fig. 6). After 2 h, replacement of the feed mixture by a flow of oxygen leads to a partial decrease of UV–vis absorbance above 600 nm (not shown); however, the EPR signal does not change, and, interestingly, the Raman band at 1033 cm^{-1} of $\nu(V^{5+}=O)$ does not reappear.

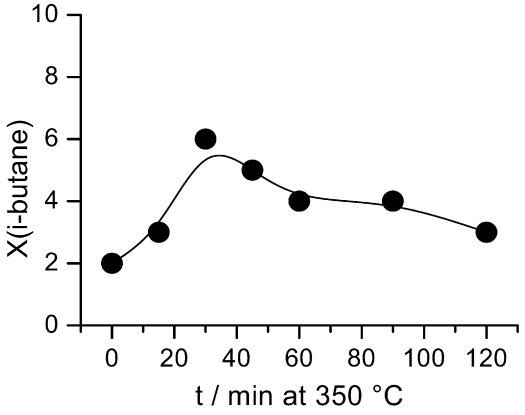

Fig. 6. Conversion of *i*-butane measured along with the spectra in Fig. 5.

3.3. Solid-state NMR studies

The ^1H MAS NMR spectra (central lines) of the as-synthesized and thermally treated samples are shown in Fig. 7. The spectrum of $H_4PVMo_{11}O_{40}\cdot 8H_2O$ can be simulated taking into account two species at 6.9 ppm (17.4%) and 7.5 ppm (82.6%) (Fig. 7a). Both species can be attributed to protons of crystal water molecules. Narrow lines together with the absence of spinning side bands support the assumption of highly mobile ^1H species in the sample between the Keggin units. The intensity and overall shape of the complete ^1H spectrum change markedly after thermal treatment at 100 °C (Fig. 7b) and again at 300 °C (Fig. 7c). The lines are significantly broader, and spinning sidebands can now be observed (not shown in Figs. 7b and 7c).

A successful fit of the experimental spectrum in Fig. 7b (after calcination at 100 °C) is obtained by superimposing six subbands from different ^1H sites. Although the overall intensity of the ^1H spectrum is decreased, the greatest contribution still arises from crystal water protons (δ_i = 7.8 ppm [63%], δ_i = 8 ppm [2%]), followed by two new species due to strongly hydrogen-bonded protons (δ_i = 9.9 ppm [25%] and

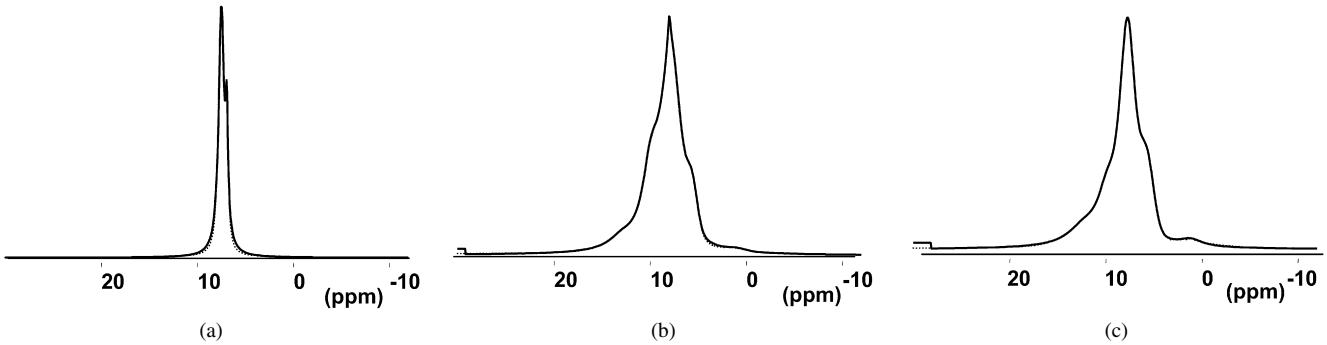

Fig. 7. ^{1}H-MAS-NMR spectra of $H_4PVMo_{11}O_{40}\cdot 8H_2O$ in as-synthesized form (a) as well as after heating in air to 100 (b) and 300 °C (c).

$\delta_i = 13$ ppm [4.5%]). The pronounced hydrogen bonding is a consequence of the decreasing void space between the Keggin units caused by the beginning dehydration. In addition, protons in isolated hydroxyl groups at surface defects ($\delta_i = 0.9$ ppm [0.5%]), as well as protons occurring in the cage of the heteropoly compound ($\delta_I = 5.6$ ppm [5%]; also see [30]) can be detected. The latter must consider the charge-compensating counter-ions of the $H_4PVMo_{11}O_{40}\cdot xH_2O$ structure. Further heating to 300 °C (Fig. 7c) leads to increased integral intensity of protons in the Keggin unit ($\delta_i = 5.7$ ppm [11.4%]) relative to the other sites, a loss of crystal water protons ($\delta_i = 7.7$ ppm [57.4%]), an increase in the protons in surface hydroxyl groups ($\delta_i = 1.2$ ppm [3%]), and the two proton sites typical for strongly bonded protons with an intensity of 28.2% ($\delta_i = 12.4$ ppm; $\delta_i = 9.8$ ppm). The overall intensity of the ^{1}H spectrum decreases again at 300 °C, however, due to the loss of crystal water.

A highly symmetric V^{5+} species with an isotropic chemical shift value of ≈−559 ppm (Fig. 8a) is detected in as-synthesized $H_4PVMo_{11}O_{40}\cdot 8H_2O$ by ^{51}V MAS NMR measurements with a spinning speed of 14 kHz. The small number of spinning sidebands indicates only marginal quadrupolar contributions. With increasing resolution using a higher spinning speed (25 kHz), two coexisting, highly symmetric V^{5+} species with chemical shift values of $\delta_{i1} = -547.6$ ppm and $\delta_{i2} = -569.8$ ppm and equal intensity can be unambiguously distinguished in $H_4PVMo_{11}O_{40}\cdot 8H_2O$ (insert in Fig. 8a). Previously, a similar signal at −580 ppm was assigned to octahedral V^{5+} in metal atom positions of the Keggin unit [7]. Static measurements of $H_4PVMo_{11}O_{40}\cdot 13$–$14H_2O$ revealed an axial signal with chemical shift tensor components at −314 ppm (⊥) and −971 ppm (‖) [6], corresponding to an isotropic mean chemical shift of −533 ppm, which agrees with the values shown in Fig. 8a as well as with those obtained previously [7]. The former axial signal has also been assigned to octahedral V^{5+} inside the Keggin units [6].

The ^{51}V spectra recorded after thermal treatments change drastically (Figs. 8b and 8c). A wide-spread manifold of spinning side bands covering several hundred kHz is observed for both spectra measured after calcination (Figs. 8b and 8c), indicating the formation of new V^{5+}-containing species with dramatically increased quadrupolar frequencies and large anisotropies of the chemical shift. After calcination at 100 °C, the newly formed species is characterized by

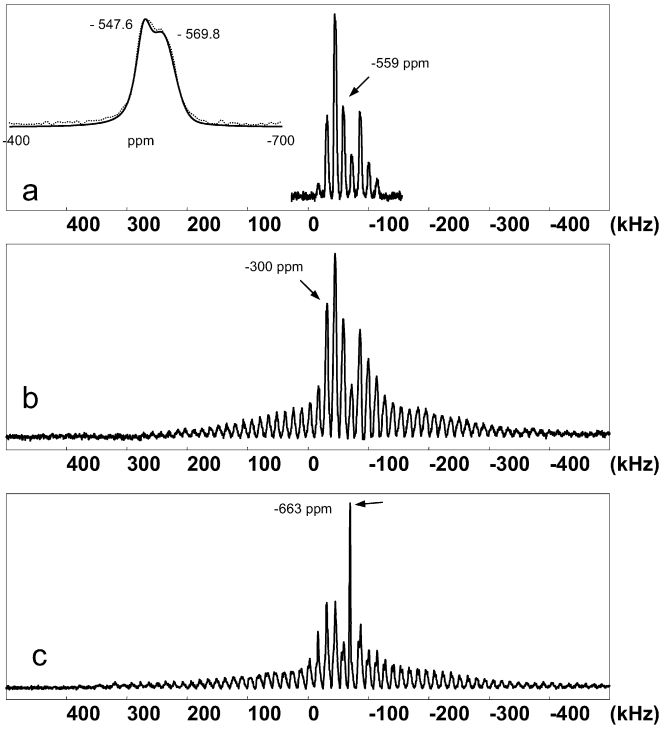

Fig. 8. ^{51}V-MAS-NMR spectra of $H_4PVMo_{11}O_{40}\cdot 8H_2O$ in as-synthesized form (a) as well as after heating in air to 100 (b) and 300 °C (c).

an isotropic chemical shift value of $\delta_I \approx -300$ ppm (Fig. 8b), whereas the new species obtained at 300 °C has an isotropic chemical shift value of $\delta_I \approx -663$ ppm (Fig. 8c).

A careful analysis of the spectra (not shown here) reveals that after calcination at 100 °C and even at 300 °C, the highly symmetric species reflected by the line at ≈−559 ppm are still present. Given that this signal is due to octahedrally coordinated V^{5+} species, which are part of the $(PVMo_{11}O_{40})^{4-}$ Keggin units, as reported previously [6], this means that even after thermal treatment up to 300 °C, a considerable part of the latter remains intact with V^{5+} sites inside.

3.4. In situ FTIR studies

Fig. 9 shows the FTIR spectra obtained during heating of $H_4PVMo_{11}O_{40}\cdot 8H_2O$ coated on a Si wafer. Spectral changes during heating in Ar flow (not shown) are almost identical.

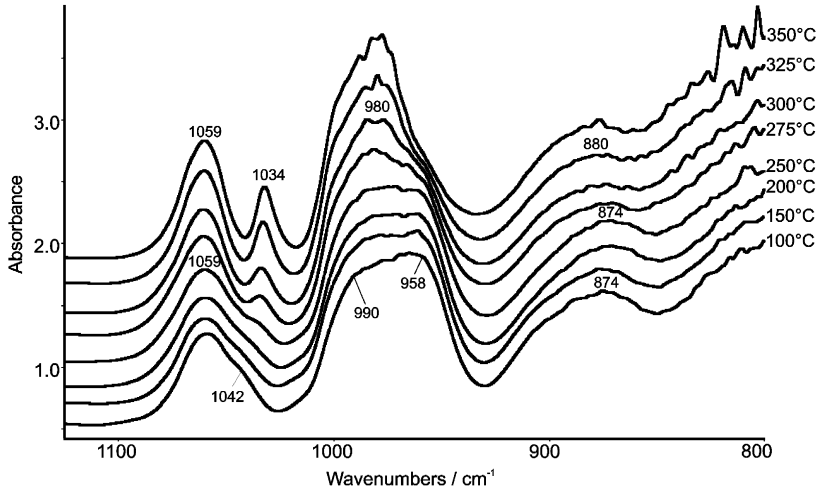

Fig. 9. FTIR spectra measured during heating of $H_4PVMo_{11}O_{40}\cdot 8H_2O$ coated on Si-wafer in air flow.

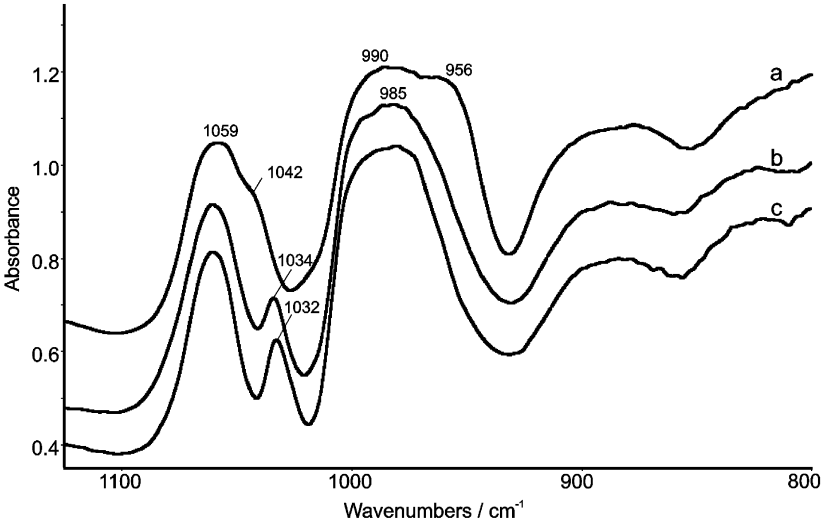

Fig. 10. FTIR spectra of $H_4PVMo_{11}O_{40}\cdot 8H_2O$ coated on Si-wafer (a) after evacuation at 25 °C, (b) after heating to 350 °C in air flow and (c) after 60 min exposure to 20% isobutane/N_2 flow and flushing with Ar at 350 °C.

The well-known and previously assigned bands of heteropolyoxometallates are as follows: ν_{as}(P–O) around 1060 cm^{-1}, ν_{as}(Mo=O) at 990–960 cm^{-1}, and ν_{as}(Mo–O–Mo) around 900–870 cm^{-1} [11,18,33,34]. Compared with the spectrum of the V-free $H_3PMo_{12}O_{40}\cdot 13H_2O$ (not shown), the asymmetric P–O and asymmetric Mo=O stretching bands are broadened and shifted to lower wavenumbers. These effects are due to decreased oxoanion symmetry caused by the substitution of one Mo in the Keggin anion by V [9,18]. Above 250 °C, a new band appears at 1034 cm^{-1} (Fig. 9), the intensity of which increases with rising temperature. Simultaneously, the shoulder of the asymmetric P–O stretching band at 1042 cm^{-1} and the shoulder of the asymmetric Mo=O stretching band at 958 cm^{-1} vanish. Only a slight shift in the ν_{as}(Mo–O–Mo) band from 874 to 880 cm^{-1} is seen. The band at 1034 cm^{-1} is also observed in samples heated up to 430 °C during thermal analysis experiments. At this temperature, the second step in the TG curve is completed, indicating destruction of the crystal water-free Keggin structure.

The band at 1034 cm^{-1} also observed during the Raman studies can be attributed to the ν(V=O) band of single $V^{5+}O_x$ [33,34]. Together with the aforementioned band changes of ν_{as}(P–O) and ν_{as}(Mo=O), the appearance of this band clearly indicates that V^{5+} has been eliminated from the Keggin anion.

When the sample is heated in isobutane/N_2 flow after pretreatment in air at 350 °C, the intensity and the half-width of the ν(V=O) band increase further (Fig. 10). In addition, a slight shift in the band position from 1034 to 1032 cm^{-1} can be seen. This shifting to lower wavenumbers points to a progressive reduction of V^{5+} to V^{4+} during isobutane exposure.

4. Discussion

4.1. Nature of the V sites in as-synthesized $H_4PVMo_{11}O_{40}\cdot 8H_2O$

Determination of the spin concentration and the spin Hamiltonian parameters in the EPR spectrum of as-synthesized

$H_4PVMo_{11}O_{40}\cdot 8H_2O$ shows that only a small fraction (2.3%) of all V sites are present as reduced $[VO(H_2O)_5]^{2+}$, ions which cannot be part of the Keggin units but rather are located in the void space between the latter (signal A, Fig. 1; Table 1).

In contrast, ^{51}V-MAS-NMR measurements compose the majority of the V sites that are pentavalent and give rise to superposition of two signals with very similar chemical shifts at −547.6 and −569.8 ppm and a low chemical shift anisotropy. A similar isotropic signal consisting of several superimposing components was observed at −580 ppm in a previous study of $H_4PVMo_{11}O_{40}$, in which the crystal water content was not given (ν_{rot} up to 15 kHz) [7]. The isotropic mean chemical shift value of $H_4PVMo_{11}O_{40}\cdot 13$–$14H_2O$ of the static axial signal measured in [6] falls in this same range. In both cases, the signals were attributed to the fact that octahedrally coordinated V^{5+} is part of the Keggin anions. The splitting has been explained by the statistical distribution of the V atoms over the 12 metal atom positions of the Keggin unit, possibly leading to differences in the local vicinity of the V atoms caused by interaction with the electric field of other V atoms located at different distances. In analogy to these results and applying higher spinning speeds ($\nu_{rot} = 25$ kHz), the lines in Fig. 8a are assigned to at least two different octahedrally coordinated V^{5+} sites within the intact Keggin anions. The intactness of most of the $(PVMo_{11}O_{40})^{4-}$ anions also is suggested by the Raman spectrum of as-synthesized $H_4PVMo_{11}O_{40}\cdot 8H_2O$ units, which shows major bands at 1002 and 256 cm^{-1} arising from the ν(Mo=O) and δ(Mo–O–Mo) vibrations of the intact Keggin moiety [13], whereas those of defective Keggin anions at 974 and 235 cm^{-1}, although also present, show much weaker intensity. Thus, the combined results of EPR, ^{51}V-MAS-NMR, and Raman spectroscopy suggest that the fresh uncalcined catalyst consists mainly of intact Keggin units in which Mo^{6+} is partially replaced by V^{5+}, with a small number $[VO(H_2O)_5]^{2+}$ ions located outside the complex anions also present.

4.2. Structural changes on thermal dehydration and treatment under catalytic conditions

Heating $H_4PVMo_{11}O_{40}\cdot 8H_2O$ to 100 °C does not change the main features of the Raman spectrum except for a shift of the ν(Mo=O) band to higher wavenumbers, which is explained by desorption of adsorbed water molecules [13]. This suggests that no further degradation of the Keggin units should occur up to 100 °C.

In the ^{51}V-MAS-MNR spectra, a new signal with a mean isotropic shift value of −300 ppm arises after heating to 100 °C, along with the initial signals at −547.6 and −569.8 ppm (Fig. 8b). The wide distribution of spinning side bands reflecting dramatically increased quadrupolar frequencies and large chemical shift anisotropies suggest that these V^{5+} species cannot be part of the Keggin units. Because the Raman results discussed earlier do not point to disintegration of V from the Keggin units in the low-temperature range (up to 100 °C), we suggest that the V^{5+} sites composed by the −300 ppm signal might have been formed by oxidation and partial dehydration of $[O{=}V(H_2O)_5]^{2+}$ species located in the void space between the Keggin units in the as-synthesized $H_4PVMo_{11}O_{40}\cdot 8H_2O$, as detected by EPR. Note that, in contrast to the simultaneous EPR/UV–vis/Raman measurements, calcination of the sample for NMR studies was done not in N_2, but in air flow, to prevent formation of V^{4+} that could disturb the NMR measurements.

In the UV–vis spectra, an intense ICVT transition appears during calcination (Fig. 4). This is a clear evidence of the shortening of the V–Mo distance, most likely by formation of V^{4+}–O–Mo^{6+} bridges. Three possibilities to account for this observation can be considered: (a) migration of $[VO(H_2O)_5]^{2+}$ (located in the void space between the Keggin anions) towards the MoO_6 octahedra, accompanied by H_2O release; (b) reduction of V^{5+} (located inside the intact Keggins), accompanied by migration out of the anion, leaving behind a defect; and (c) reduction of V^{5+} (located inside the intact Keggins) without migration and defect formation. Variant (c) is not supported by the experimental data. If no defect formation occurred, then the positions of Raman and FTIR bands should not change; however, this did occur in Figs. 3 and 9. The spin Hamiltonian parameters of EPR signals B and C arising from reduced $V^{4+}O_6$ species at 100 °C are still well within the range of octahedral V^{4+} (Fig. 2, Table 1), however the markedly larger $\Delta g_{\parallel}/\Delta g_{\perp}$ values point to larger distortion derived from signal A due to changes in the local V coordination. This could be caused by the stepwise loss of water ligands from $[O{=}V(H_2O)_5]$ outside the Keggin units, as follows:

$$\underset{\text{EPR signal A}}{[O{=}V(H_2O)_5]} \rightarrow \underset{\text{EPR signals B and C}}{[O{=}VO_x(H_2O)_{5-x}]} \rightarrow \underset{\text{EPR signal D}}{[O{=}VO_4]}. \quad (2)$$

The simultaneously increasing ICVT transition reflecting the formation of V^{4+}–O–Mo^{6+} bridges suggests that sequence (2) is accompanied by stepwise condensation of the initial $[O{=}V(H_2O)_5]$ to the outer surface of the Keggin anions. In the final state of dehydration (sequence 2, signal D), the V^{4+} sites achieve a square-pyramidal coordination, as suggested by the spin Hamiltonian parameters of signal D (Fig. 2, Table 1). This does not agree with the location of V^{4+} in octahedral sites of intact Keggin units and supports the conclusion that reduced V^{4+} cannot be part of the latter. Thus, it must be concluded that V^{4+}–O–Mo^{6+} bridges as evidenced by the ICVT transitions are formed by migration and attachment of extra-Keggin V^{4+} to the surface of the Keggin units, and also likely by reduction of V^{5+} in Keggin positions, accompanied by migration out of the anion, leaving behind a defect, because the total percentage of V^{4+} increases during thermal treatment and even more during the catalytic reaction. Defect formation is suggested by a shift in the δ(Mo–O–Mo) Raman band to a value well below 255 cm^{-1} (Fig. 2).

In the ^{51}V-NMR spectrum, an isotropic signal at −663 ppm arises after calcination at 300 °C. In addition, isotropic signals at ca. −660 ppm were reported after thermal treatment of $H_4PVMo_{11}O_{40}\cdot xH_2O$ at 280 °C [6] and 320 °C [7,31]; these were assigned to tetrahedrally coordinated V^{5+} extracted from the Keggin anion. However, it must be mentioned that the chemical shift value of a V^{5+} site in such heteropolyacids seems to be only weakly dependent on the number of O atoms in its first coordination sphere. In fact, a chemical shift of −549 ppm,

very close to that observed for octahedral V^{5+} within the Keggin units of as-synthesized $H_4PVMo_{11}O_{40}\cdot 8H_2O$ (Fig. 8a), was found for the $(VMo_{12}O_{40})^{3-}$ anion and assigned to V in the tetrahedral heteroatom position in the centre of the Keggin unit [32]. Thus, the exact local geometry of the V^{5+} sites contributing to the −663 ppm signal in Fig. 8c cannot be deduced simply from the chemical shift. However, considering the Raman data indicating the formation of defective Keggin units and EPR results that point to removal and condensation of $O_4V^{4+}{=}O$ moieties on the surface of the Keggin units, it seems plausible to assign the signal at −663 ppm in Fig. 8c to V^{5+} species that also were extracted from the Keggin units but were not reduced due to calcination in air instead of N_2. The fact that, along with the signal at −663 ppm, the original line at ≈−559 ppm is still observed even after calcination at 350 °C indicates that not all V sites are removed from the Keggin units.

On heating the calcined catalyst in 11% isobutane and 17.7% O_2/N_2 flow, slight further reduction of V^{5+} to V^{4+} occurs and reaches equilibrium at 350 °C. Isobutane conversion increases during the first 40 min time on stream at 350 °C. This may coincide with the formation of active sites, that is, disintegration of V sites and condensation on the surface of the Keggin anions. This may improve their accessibility. No serious damage to the crystal structure or Keggin units was observed under these conditions. Nevertheless, activity was found to decrease in due course (Fig. 6). This is certainly not due to the reduction of V^{5+} to V^{4+}, because this reaches equilibrium well before the onset of activity drop. A more probable reason for the decreased activity may be the accumulation of carbon-containing deposits on the catalyst surface, which contribute to the UV–vis absorbance above 600 nm. These deposits can be removed by treatment in O_2 flow at 330 °C; however, reoxidation of the VO^{2+} species is not possible at this temperature. This activity loss was not observed in actual catalytic tests, in which a MAC selectivity of 30% was reached at a conversion of 35%. However, in this case, large amounts of water vapour were added to the feed, which was not done in the in situ-spectroscopic experiments in this study.

5. Conclusion

The integrated in situ-spectroscopic approach adopted in this work revealed that the vast majority of the V species in as-synthesized $H_4PVMo_{11}O_{40}\cdot 8H_2O$ are pentavalent and part of the Keggin anions, along with a small percentage (2.3%) of V sites residing in the void space of the crystal structure as $[VO(H_2O)_5]^{2+}$ ions. On thermal treatment in N_2 or air, stepwise release of water ligands from those ions (and partial oxidation in air) finally leads to square-pyramidal $O{=}V^{4+/5+}O_4$ species attached by four V–O–Mo bridges to the surface of a Keggin anion. In addition, further disintegration of V^{5+} from the intact Keggin units occurs on complete crystal water removal above ≈200 °C, possibly followed by further reduction to V^{4+}, depending on nature of the atmosphere under which the thermal treatment is performed. This leaves behind defective Keggin moieties. However, no serious damage of the $H_4PVMo_{11}O_{40}$ structure is observed during gentle calcination in N_2 and air or even during catalytic treatment in isobutane/O_2/N_2 flow up to 350 °C.

Comparing the EPR, ^{51}V-NMR, and FTIR results suggests that at temperatures relevant for isobutane oxidation, pentavalent V exists in both intra- and extra-Keggin positions, whereas tetravalent V is obviously not stable within the Keggin units. This means that not only the temperature, but also the reducing power of the atmosphere in which the sample is treated, forces the V sites to leave the Keggin moiety. Treatment in the reactant mixture used for isobutane oxidation obviously provides rather mild reducing conditions leading to a reduction (and disintegration) of only 32% of all V sites, while Mo sites remain essentially hexavalent. This differs markedly from conditions during methanol oxidation, which lead to deeper V reduction and even to the formation of Mo^{5+} [12]. Both effects could favor a more rapid loss of catalyst stability.

As a consequence of the results described above and in agreement with previous work, it can be concluded that the active state of the catalyst is formed by a dynamic restructuring process during the initial reaction period. Under the conditions applied in this work, this process does not lead to a marked change in the $H_4PVMo_{11}O_{40}$ crystal structure, but does lead to the formation of defects in the Keggin units. The spectroscopic results suggest that these defects are formed by partially removing V from the latter. However, the possibility that Mo is partially removed, too, cannot be excluded. In any case, despite the resulting defects, the crystal structure of $H_4PVMo_{11}O_{40}$ remains widely intact under the conditions used in this work. Note that this may be different when other reaction conditions are used (e.g., higher reaction temperature and/or stronger reducing reactants). During calcination and isobutane oxidation, extra-Keggin $O{=}VO_4$ species attach to the surface of these complex anions, thereby forming $V^{4+/5+}$–O–Mo^{6+} single sites. Although V-free heteropolyacids do also catalyze selective isobutane oxidation, structures containing vanadium are generally more active [8]. Thus, the aforementioned $V^{4+/5+}$–O–Mo^{6+} single sites are considered the active ones in $H_4PVMo_{11}O_{40}$. Further work is dedicated to the development of catalysts with an increased concentration of this type of site to enhance activity while maintaining selectivity to MAC and MAA.

Acknowledgments

The authors thank the German Federal Ministry of Education and Research for financial support (grant 03X2001B).

References

[1] N. Mizuno, M. Misono, Chem. Rev. 98 (1998) 199.
[2] L. Marosi, G. Cox, A. Tenten, H. Hibst, J. Catal. 194 (2000) 140.
[3] L. Marosi, C. Otero Areán, J. Catal. 213 (2003) 235.
[4] A. Aboukais, C. Haubtmann, J.J. André, C. Desquilles, M. Dourdin, I. Mathes-Juventin-Andrieu, F.C. Aissi, M. Guelton, J. Chem. Soc. Faraday Trans. 91 (1995) 1025.
[5] Th. Ilkenhans, B. Herzog, Th. Braun, R. Schlögl, J. Catal. 153 (1995) 275.
[6] E. Blouet-Crusson, M. Rigole, M. Fournier, A. Aboukais, F. Daubrege, G. Hecquet, M. Guelton, Appl. Catal. A Gen. 178 (1999) 69.
[7] C. Marchal-Roch, R. Bayer, J.F. Moisan, A. Tézé, G. Hervé, Top. Catal. 3 (1996) 407.

[8] F. Cavani, R. Mezzogori, A. Pigamo, F. Trifirò, E. Etienne, Catal. Today 71 (2001) 97.
[9] M. Sultan, S. Paul, M. Fournier, D. Vanhove, Appl. Catal. A Gen. 259 (2004) 141.
[10] J. Melsheimer, S.S. Mahmoud, G. Mestl, R. Schlögl, Catal. Lett. 60 (1999) 103.
[11] J.K. Lee, J. Melsheimer, S. Berndt, G. Mestl, R. Schlögl, K. Köhler, Appl. Catal. A Gen. 214 (2001) 125.
[12] J.K. Lee, V. Russo, J. Melsheimer, K. Köhler, R. Schlögl, Phys. Chem. Chem. Phys. 2 (2000) 2977.
[13] G. Mestl, T. Ilkenhans, D. Spielbauer, M. Dieterle, O. Timpe, J. Kröhnert, F. Jentoft, H. Knözinger, R. Schlögl, Appl. Catal. A Gen. 210 (2001) 13.
[14] T. Ressler, O. Timpe, F. Girsdies, J. Wienhold, T. Neisius, J. Catal. 231 (2005) 279.
[15] F.C. Jentoft, S. Klokishner, J. Kröhnert, J. Melsheimer, T. Ressler, O. Timpe, J. Wienhold, R. Schlögl, Appl. Catal. A Gen. 256 (2003) 291.
[16] A. Pöppl, P. Manikandu, K. Köhler, P. Maas, P. Strauch, R. Böttcher, D. Goldfarb, J. Am. Chem. Soc. 123 (2001) 4577.
[17] A. Brückner, Chem. Commun. (2005) 1761.
[18] B.B. Bardin, R.J. Davis, Appl. Catal. A Gen. 185 (1999) 283.
[19] G.P. Lozos, B.M. Hofman, C.G. Franz, Quantum Chemistry Programs Exchange (1973) No. 265.
[20] ICSD database, entry no. 31128.
[21] D.G. Cory, W.M. Ritchey, J. Magnet. Res. 80 (1988) 128.
[22] D. Massiot, F. Fayon, M. Capron, I. King, S. Le Calvé, B. Alonso, J.O. Durand, B. Bujoli, Z. Gan, G. Hoatson, Magn. Reson. Chem. 40 (2002) 70.
[23] B. Bayer, C. Marchal, F.X. Liu, A. Tézé, G. Hervé, J. Mol. Catal. A Chem. 110 (1996) 65.
[24] S. Klokishner, J. Melsheimer, R. Ahmad, F.C. Jentoft, G. Mestl, R. Schlögl, Spectrochim. Acta A 58 (2002) 1.
[25] K. Nowinska, A.B. Wieckowski, Z. Phys. Chem. Neue Folge 162 (1989) 231.
[26] A. Davidson, M. Che, J. Phys. Chem. 96 (1992) 9909.
[27] G.T. Wendt, L.-J. Leu, A.T. Bell, J. Catal. 134 (1992) 479.
[28] L.J. Burcham, G. Deo, X. Gao, I.E. Wachs, Top. Catal. 11/12 (2000) 85.
[29] G.G. Cortez, M.A. Bañares, J. Catal. 209 (2002) 197.
[30] M. Fait, D. Heidemann, H.-J. Lunk, Z. Anorg. Allg. Chem. 625 (1999) 530.
[31] B. Taouk, D. Ghoussoub, A. Bennani, E. Crusson, M. Rigole, A. Aboukais, R. Decressain, M. Fournier, M. Guelton, J. Chim. Phys. 89 (1992) 435.
[32] S. Himeno, T. Osakai, A. Saito, Bull. Chem. Soc. Jpn. 64 (1991) 21.
[33] N. Mizuno, D.-J. Suh, W. Han, T. Kudo, J. Mol. Catal. A Chem. 114 (1996) 309.
[34] X.-K. Li, J. Zhao, W.-J. Ji, Z.-B. Zhang, Y. Chen, C.-T. Au, S. Han, H. Hibst, J. Catal. 237 (2006) 58.